Surface and Structure Characterization of Some Perovskite-Type Powders To Be Used as Combustion Catalysts

Marco Daturi and Guido Busca*

Istituto di Chimica, Facoltà di Ingeneria, Università, P. le J. F. Kennedy, I-16129 Genova, Italy

Ronald J. Willey

Department of Chemical Engineering, Northeastern University, Boston, Massachusetts 02115

Received May 2, 1995. Revised Manuscript Received July 10, 1995[⊗]

Some perovskite-type transition-metal mixed oxide powders active in the combustion catalysis, with formulas $LaMO_3$ (M = Fe, Cr, Co, and Mn), have been prepared by different methods. Similarly, potential supports for combustion catalysts nearly isostructural with the above ones have been prepared, with compositions $SrZrO_3$ and $LaAlO_3$. Mixed phases with formulas $Sr_{1-x}La_xZr_{1-x}Mn_xO_3$ have also been investigated. The bulk properties have been studied by XRD, far-IR spectroscopy, and DTA-TG analyses. Morphological properties have been determined by XRD, SEM, and surface area measurements. These phases crystallize after heating at 970 K (except $LaFeO_3$, which is already crystalline after calcination at 770 K) with surface area ranging 10–20 m^2/g. The solubility of $LaMnO_3$ into $SrZrO_3$ is limited to near 10%. Their surface properties have been investigated by IR spectroscopy that showed a predominantly basic surface character of all these solids.

Introduction

The catalytic combustion technologies represent possible solutions to different air pollution problems. The catalytic combustion of hydrocarbons, such as methane or natural gas, aimed to the energy production gives rise to lower temperatures with respect to thermal combustion, so limiting the production of NO_x.[1,2] Nevertheless, one of the requirements for the development of this technology is the availability of catalytically active materials stable at very high temperatures (up to 1500 °C) and, possibly, free from the very expensive and quite unstable noble metals.[3]

Less stringent requirements are needed to be fulfilled for combustion catalysts aimed to the abatement of volatile organic compounds (VOC)[4,5] including those used for destroying the emissions from industrial chemical plants[6] and unburned residues from automotive waste gases in catalytic converters.[7] Also for these applications, the use of transition metal-based catalysts is possible.

As for the catalytically active phases, lanthanum metalates such as $LaMnO_3$, $LaCoO_3$, $LaFeO_3$, and $LaCrO_3$ have been found to exhibit very high combustion catalytic activity,[8–13] comparable to those of noble-metal-based catalysts. The structures of such compounds are strongly related, being all constituted by distorted perovskite-like lattices. On the other hand, several different ceramic materials have been found to be promising as supports or washcoats for catalytic combustion catalysts. Among them, the perovskite-like phases $SrZrO_3$ and $LaAlO_3$ appear quite interesting, because some data in the literature indicate a high stability towards sintering at high temperatures.[14,15]

To develop new combustion catalysts, the compatibility of the active phases with the supports must be checked. Moreover, the knowledge of the surface properties of these materials is also hopeful. Nevertheless, relatively few data are reported in the literature concerning the surface properties of perovskite-based powders.[16–18]

For these reasons, we undertook the preparation and characterization of perovskite-like powders that are

[⊗] Abstract published in *Advance ACS Abstracts,* August 15, 1995.

(1) Prasad, R.; Kennedy, L. A.; Ruckenstein, E. *Catal. Rev. Sci. Eng.* **1984**, *26*, 1.
(2) Pfefferle, L. D.; Pfefferle, W. C. *Catal. Rev. Sci. Eng.* **1987**, *29*, 219.
(3) Zwinkels, M. F. M.; Jaras, S. G.; Menon, P. G.; Griffin, T. A. *Catal. Rev. Sci. Eng.* **1993**, *35*, 319.
(4) Spivey, J. J. *Ind. Eng. Chem. Res.* **1987**, *26*, 2165.
(5) Spivey, J. J. In *Catalysis*; The Royal Society of Chemistry: Cambridge, 1989; Vol. 8, p 158.
(6) Laudonia, L.; Leonetti, U. *Chim. Ind. (Milan)*, **1994**, *76*, 656.
(7) Taylor, K. C. In *Catalysis Science and Technology*; Anderson, J. R., Boudart, M., Eds.; Springer-Verlag: Berlin, 1984; Vol. 5, p 119.
(8) Tejuca, L. G.; Fierro, J. L. G.; Tascon, J. M. D. *Adv. Catal.* **1989**, *36*, 237.
(9) Carberry, J. J.; Rajadurai, S.; Alcock, C. B.; Li, B. *Catal. Lett.* **1990**, *4*, 43.
(10) Tabata, K.; Misono, M. *Catal. Today* **1990**, *8*, 249.
(11) Seiyama, T. *Catal. Rev. Sci. Eng.* **1992**, *34*, 281.
(12) Seiyama, T.; In *Properties and Applications of Perovskite-type Oxides*; Tejuca, L. G., Fierro, J. L. G., Eds.; Dekker: New York, 1993; p 215.
(13) Marti, P. E.; Baiker, A. *Catal. Lett.* **1994**, *26*, 71.
(14) Lowe, D. M.; Gusman, M. I.; McCarty, J. G.; In *Preprints of the VIth Int. Symp. on Preparation of Catalysts*; Louvain la Neuve, Belgium, 1994; Vol. 2, p 39. Quinlan, M. A.; Wise, H.; McCarty, J. G. *Basic research on natural gas combustion phenomena-catalytic combustion*; SRI International: Menlo Park, CA, GRI-89/0141, 1989, cited in ref 3.
(15) Marti, P. E.; Maciejewski, M.; Baiker, A.; In *Preprints of the VIth Int. Symp. on Preparation of Catalysts*; Louvain la Neuve, Belgium, 1994; Vol. 2, p 211.
(16) Tascon, J. M. D.; Fierro, J. M. G.; Tejuca, L. G. In *Properties and Applications of Perovskite-type Oxides*; Tejuca, L. G., Fierro, J. L. G., Eds.; Dekker: New York, 1993; p 215.

0897-4756/95/2807-2115$09.00/0

possible candidates for supports and active phases of performant and stable catalytic combustion catalysts.

Experimental Section

Preparation Procedures. The samples of $LaCoO_3$, $LaMnO_3$, $LaAlO_3$, and $SrZrO_3$ have been prepared via a conventional coprecipitation method, mixing carefully and solubilizing in water stoichiometric amounts of the precursors; later the solution was taken to pH = 10 by adding $(NH_4)_2CO_3$, then it has been left aging overnight; finally, water was evaporated, the obtained cake has been dried by heating at 393 K for 3 h and later calcined in air at different temperatures.

The precursors were $La(NO_3)_3{\cdot}6H_2O$, $Co(NO_3)_2{\cdot}6H_2O$, $Mn(CH_3COO)_2{\cdot}4H_2O$, $Al(NO_3)_3{\cdot}9H_2O$ (all from Carlo Erba, Milan, Italy), $Sr(OH)_2{\cdot}8H_2O$ (Strem Chemicals), and $Zr(CH_3COCH{=}COCH_3)_4$ (Aldrich). A commercial $SrZrO_3$ (Strem) was also investigated.

$LaCrO_3$ and $LaFeO_3$ have been prepared as aerogels via the so-called supercritical drying technique, starting from lanthanum(III) acetate hydrate, iron(III), and chromium(III) acetylacetonate (Aldrich), in methanolic solution. The salts were hydrolyzed with stoichiometric amounts of water and dried at 523 K and 11 721 MPa, i.e., under supercritical conditions (T_c = 512.6 K; P_c = 8096 MPa for methanol).

Characterization Techniques. The XRD spectra have been recorded on a Philips PW 2256/20 diffractometer (Co Kα radiation, Ni filter; 40 kV, 20 mA). Cell parameters have been calculated by dedicated least-squares software. The crystal size was evaluated by using Scherrer's formula.[19]

The IR spectra were recorded by a Nicolet Magna 750 Fourier transform instrument. The skeletal spectra in the region above 400 cm^{-1} have been recorded with KBr pressed disks and with a KBr beam splitter, while those in the far infrared region (400–50 cm^{-1}) have been recorded using the powder deposited on polyethylene disks and with a "solid substrate" beam splitter.

The adsorption experiments were performed using pressed disks of the pure powders, activated by outgassing at 300–1070 K into the IR cell.

The BET surface areas have been measured by a sorptometer Perkin Elmer 212 C by measuring the adsorption of nitrogen at 77 K.

DTA-TG experiments were performed with a Setaram TGA 92 12 apparatus, from room temperature to 1000 °C, with a heating and cooling rate of 10 K/min.

Results

Preparation and Characterization of Lanthanum Transition Metalates $LaMO_3$ Powders. The XRD patterns of the powders as prepared or calcined at temperatures lower than 773 K do not present any evidence of crystalline mixed oxide phases, either being completely flat due to amorphous materials or showing the presence of hydroxides and/or carbonate phases.

In Figure 1 the DTA and DTG curves relative to the calcination of the $LaMO_3$ materials are reported in the region above 773 K. Below this temperature decomposition reactions are found in all cases, with relevant weight losses. Above this temperature the DTG traces of all materials show small weight losses associated with a weak endothermic peak, centered in the range 1020–1100 K depending on the countercation M^{3+}. These

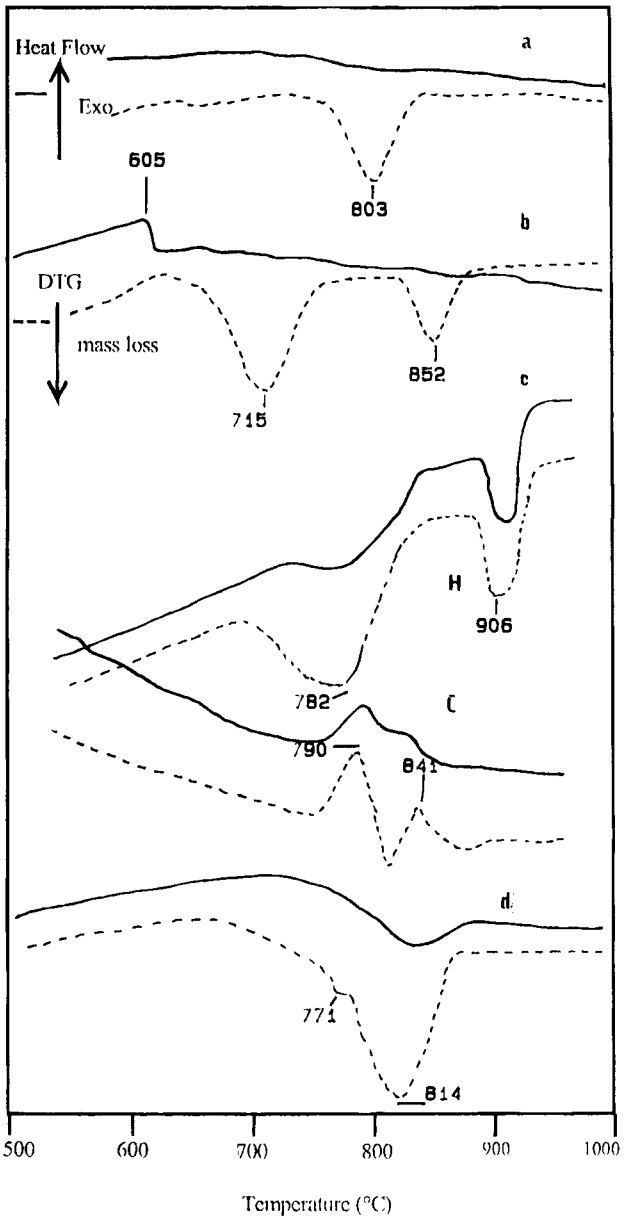

Figure 1. DTA (full lines) and DTG (dashed lines) curves relative to $LaFeO_3$ (a), $LaCrO_3$ (b), $LaCoO_3$ (c), and $LaMnO_3$ (d) samples, previously calcined at 773 K, in the 773–1273 K range. For $LaCoO_3$ the curves recorded both during heating (H) and during cooling (C) are reported.

phenomena are attributed to the decomposition of carbonate species, according to the IR data discussed below. We can mention that, according to previous literature data, also "pure" lanthana La_2O_3 is easily carbonated at ambient atmosphere[20] and this characterizes our powders, and lanthana, as strongly basic materials. Experiments with home-prepared $La_2O_2CO_3$ seem to exclude a role of this phase in determining the features in the range 1020–1100 K of the DTA-TG curves.

In the cases of $LaFeO_3$ and $LaMnO_3$ no other features are observed. In the case of $LaCrO_3$ a pronounced exothermic peak, assigned according to the XRD data discussed below to the crystallization of the perovskite phase, is observed near 880 K. Moreover, an additional

(17) Fierro, J. L. G. In *Properties and Applications of Perovskite-type Oxides*; Tejuca, L. G., Fierro, J. L. G., Eds.; Dekker: New York, 1993; p 195.
(18) Busca, G.; Buscaglia, V.; Leoni, M.; Nanni, P. *Chem. Mater.* **1994**, *6*, 955.
(19) West, A. R. *Solid State Chemistry and Its Applications*, Wiley: New York, 1984.
(20) Bernal, S.; Botana, F. J.; Garcia, R.; Pintado, J.; Rodriguez Izquierdo, J. M. *J. Less Common Met.* **1985**, *110*, 433.

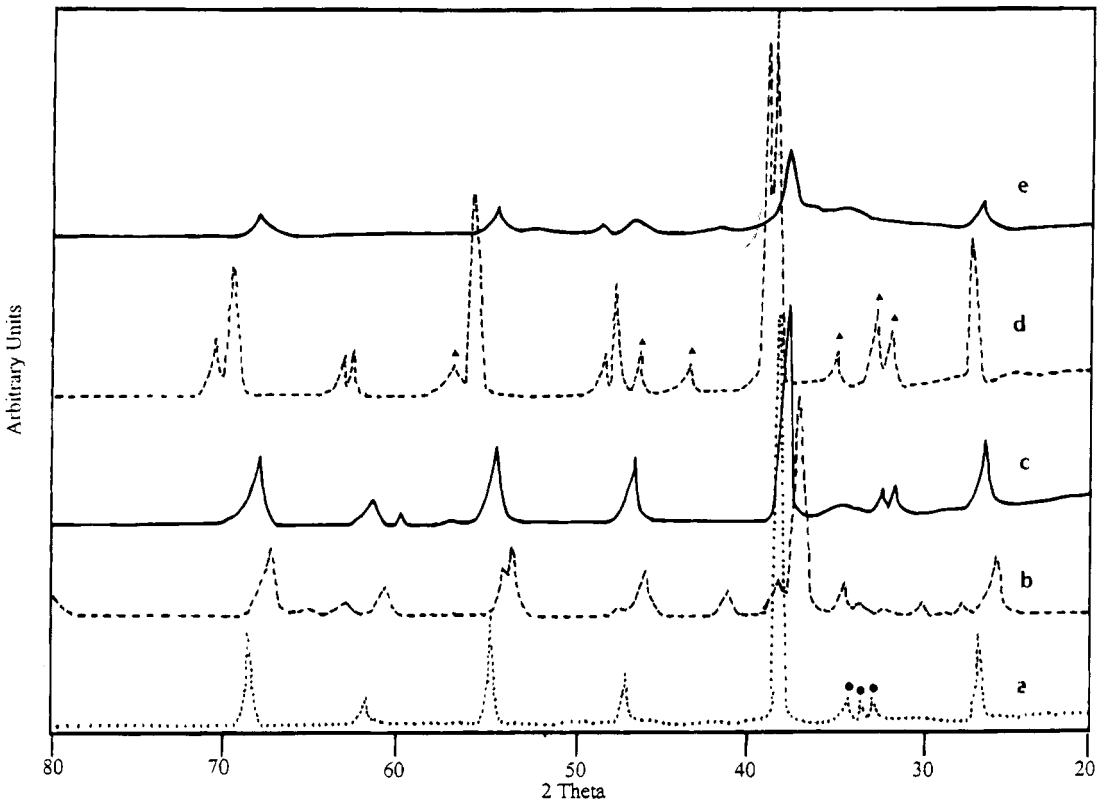

Figure 2. XRD powder diffraction patterns of $LaCrO_3$ (a), $LaFeO_3$ (b), $LaMnO_3$ (c), and $LaCoO_3$ (d) samples, all calcined at 973 K. (e) $LaFeO_3$ calcined at 773 K. The circles in (a) represent peaks of La_2CrO_6 phase, while the triangles in (d) show features of La_2CO_5.

weight loss is observed near 980 K, and this can be assigned to the decomposition of La_2CrO_6, identified by XRD and IR analyses. In the case of $LaCoO_3$ an additional weight loss is observed near 1180 K, associated with a pronounced endothermic peak. Corresponding exothermic peak and weight gain are found near 1080 K upon cooling. This indicates that a reversible decomposition occurs, likely associated with the conversion of Co_3O_4 impurities to CoO, known to occur in this temperature range.[21]

In Figure 2 the XRD diffraction patterns of the $LaMO_3$ powders with M = Fe, Cr, Co, and Mn, all calcined at 973 K are reported. For the sample $LaFeO_3$ the pattern after calcination at 773 K is also shown. In fact this sample is the only one that shows the perovskite pattern after calcination at so low a temperature, according to DTA data that do not show crystallization peaks above 773 K. All other samples are completely amorphous after calcination at 773 K.

In Table 1 the unit cell parameters of the perovskite-like phases calculated from the patterns of the samples calcined at 973 K are compared with those reported in the literature, and a good agreement can be found.

In the cases of $LaCrO_3$ and $LaFeO_3$ the features of the orthorhombic perovskite structure are predominant (compare with JCPDS Tables 33-701 and 37-1493). This is the so-called "$GdFeO_3$ structure"[22] belonging to the $Pnma = D_{2h}^{16}$ space group, with four formula units per unit cell, so containing four subunits with the ABO_3 stoichiometry, corresponding to the unit cell of the cubic perovskite structure but with the M ion in corner-sharing distorted octahedra and lanthanum ions with 8-fold coordination only (with respect to 12-fold coordination in cubic perovskite).

The detection of this phase is not surprising in the case of the ferrite and the chromite. According to the literature, in fact, this is the stable phase at room temperature for both lanthanum orthoferrite and orthochromite, with phase transitions at near 1250 K and near 540 K to rhombohedral structures, respectively.[23] The XRD pattern of our $LaCoO_3$ sample agrees with that reported in the literature (JCPDS Table 25-1060) and is due to a hexagonal–rhombohedral phase, originally considered to belong to the $R\bar{3}m$ space group. However, it has more recently been recognized that this phase belongs to the space group $R\bar{3}c = D_{3d}^6$ with $Z = 2$,[24] which can convert to another hexagonal structure ($R\bar{3}$ space group) by segregation of low- and high-spin cobalt ions above 400 K.[25] The rhombohedral structure of $LaCoO_3$ is obtained from the ideal cubic perovskite structure by a tilting of adjacent BO_6 octahedra along the c axis. So, the O atoms lay on a C_2 axis from the D_{4h} site symmetry that have in cubic perovskite. The Co–O–Co are symmetric (with equal Co–O distances) but bent. Due to these distortions, the primitive unit cell is expanded to contain two molecular units instead of one and the overall coordination at lanthanum is 6-fold.[25]

(21) Narducci, D.; Negroni, F.; Mari, C. M. *Mater. Chem. Phys.* **1985**, *12*, 377.
(22) Hyde, B. G.; Andersson, S. *Inorganic Crystal Structures*; Wiley: New York, 1989.
(23) Landolt-Bornstein, *Numerical Data and Functional Relationships In Science and Technology*; Springer-Verlag: Berlin, 1970; Vol. III/4a.
(24) Thornton, G.; Tofield, B. C.; Hewat, A. W. *J. Solid State Chem.* **1986**, *61*, 301.
(25) Arunarkavalli, T.; Kulkarni, G. U.; Rao, C. N. R. *J. Solid State Chem.* **1993**, *107*, 299.

Table 1. Space Group, Cell Parameters, and Impurity Phases in Perovskite-like Samples[a]

sample	calcination T	space group	XRD phase	cell parameters (Å) a	b	c	impurities	ref
$LaFeO_3$	973 (1.5)	*Pnma* D_{2h}^{16} $z = 4$	O	5.603 (5)	7.857 (4)	5.561 (7)		tw
		Pnma D_{2h}^{16} $z = 4$	O	5.5669 (4)	7.8547 (7)	5.5530 (8)		*b*
$LaCrO_3$	973 (1.5)	*Pnma* D_{2h}^{16} $z = 4$	O	5.483 (4)	5.525 (4)	7.783 (4)	La_2CrO_6	tw
		Pnma D_{2h}^{16} $z = 4$	O	5.479	5.513	7.756		*c*
$LaMnO_x$	973 (3)	$R\bar{3}c$ D_{3d}^{6} $z = 2$	H	5.534 (2)		13.363 (8)		tw
$LaMnO_{3.15}$		$R\bar{3}c$ D_{3d}^{6} $z = 2$	H	5.523		13.324		*d*
$LaCoO_3$[g]	973 (3)	$R\bar{3}m$ D_{3d}^{5} $z = 2$	H	5.454 (2)		13.135 (9)	La_2CO_5 (Co_3O_4)	tw
		$R\bar{3}m$ D_{3d}^{5} $z = 2$	H	5.441		13.088		*e*
$LaAlO_3$	973 (3)	$R\bar{3}m$ D_{3d}^{5} $z = 2$	H	5.356 (3)		13.163 (17)	La_2O_3	tw
		$R\bar{3}m$ D_{3d}^{5} $z = 2$	H	5.364		13.11		*f*

[a] H = hexagonal; O = orthorhombic. tw = this work. [b] JCPDS 37-1493. [c] JCPDS 33-701. [d] JCPDS 32-484. [e] JCPDS 25-1060. [f] JCPDS 31-22. [g] According to more recent data (refs 24 and 25) the correct space group for $LaCoO_3$ is $R\bar{3}c$ D_{3d}^{6}, $z = 2$.

The XRD pattern of our $LaMnO_3$ sample is similar to those of $LaFeO_3$ and $LaCrO_3$, previously discussed. In the case of $LaMnO_3$ it is well-known that the structural distortion depends on oxygen content. For rigorously stoichiometric $LaMnO_3$ the cell is orthorhombic,[26] isostructural with $LaFeO_3$ and $LaCrO_3$ (JCPDS Tables 33-713 and 35-1353), but high-temperature syntheses generally produce nonstoichiometric oxygen-excess phases with rhombohedral–hexagonal unit cell (JCPDS 32-484), isostructural with $LaCoO_3$.[27]

One of the most sensitive features to distinguish rhombohedral from orthorhombic structure is the multiplicity of the diffraction near $d = 2.75$ Å ($2\theta \cong 38°$). In the case of the orthorhombic structure, we expect actually a triplet (with the most intense peak in the middle due to the (200), (112) reflections, and smaller peaks at lower d and at higher d, due to (021) and (020) planes, respectively). In the case of the rhombohedral structure, instead, we expect a strong doublet, with two components of nearly equivalent intensities, due to the (110) and (104) planes. In effect, this splitting is very evident in the XRD pattern of our $LaCoO_3$ sample.

The pattern of our $LaMnO_3$ sample shows not this splitting but apparently a single but rather broad peak. This fact and the rather low relative intensity of the peak due to the (024) planes seem to suggest a coexistence of both orthorhombic and rhombohedral phases, with an excess of oxygen in our sample. In Table 1 the cell parameters calculated assuming a rhombohedral structure are reported, because those obtained assuming an orthorhombic structure have a higher standard deviation.

We must however notice that the above XRD patterns provide evidence the presence of impurities in some samples. The $LaCrO_3$ powder pattern shows the presence of the chromate La_2CrO_6 as an impurity together with the main orthorhombic perovskite phase. The detection of this phase in the sample calcined at 973 K apparently contrasts the detection of its decomposition peak in the DTA experiments just near 980 K. This could be associated to the only partial decomposition of this species during calcination or, more probably, to a partial reversibility of this process. In the case of the $LaCoO_3$ sample the main impurity is the lanthanum oxycarbonate La_2CO_5 (JCPDS Tables 23-320 and 23-322) while Co_3O_4, whose presence is suggested by both DTA and FT-IR measurements, is apparent in traces, if any. The $LaMnO_3$ and $LaFeO_3$ phases are virtually pure.

In Figure 3 the skeletal IR spectra of the $LaFeO_3$, $LaCrO_3$, $LaCoO_3$, and $LaMnO_3$ samples are reported. The vibrational structures of these perovskite phases have been analyzed previously by Couzi and Huong.[28] According to the factor group analysis, the irreducible representation for the optical modes of the orthorhombic phase (D_{2h}^{16} space group) is

$$\Gamma_{opt} = 7A_g(R) + 7B_{1g}(R) + 5B_{2g}(R) + 5B_{3g}(R) + 8A_u(\text{inactive}) + 7B_{1u}(IR) + 9B_{2u}(IR) + 9B_{3u}(IR)$$

while for the rhombohedral phase (D_{3d}^{6} space group) is

$$\Gamma_{opt} = A_{1g}(R) + 3A_{2g}(\text{inactive}) + 4E_g(R) + 2A_{1u}(\text{inactive}) + 3A_{2u}(IR) + 5E_u(IR)$$

This implies that the IR spectrum for the orthorhombic phase (25 IR-active modes) is expected to be more complex than that of the rhombohedral one (8 IR active modes). However, the complexity of the spectra of our $LaMO_3$ powders (Figure 3) does not seem very different. All spectra agree with those reported in the literature for the corresponding compounds.[28–32] They show three

(26) Elemans, J. B. A. A.; van Laar, B.; van der Veen, K. R.; Loopstra, B. O. *J. Solid State Chem.* **1971**, *3*, 238.
(27) Van Roosmalen, J. A. M.; Cordfunke, E. H. P.; Helmholdt, R. B.; Zandbergen, H. W. *J. Solid State Chem.* **1994**, *110*, 100.
(28) Couzi, M.; van Huong, P. *J. Chim. Phys.* **1972**, 1339.
(29) Subba Rao, V.; Rao, C. N. R.; Ferraro, J. R. *Appl. Spectrosc.* **1970**, *24*, 436.
(30) Ganguly, P.; Vasanthacharya, N. Y. *J. Solid State Chem.* **1986**, *61*, 164.
(31) Tajima, S.; Masaki, A.; Uchida, S.; Matsuura, T.; Fueki, K.; Sugai, S. *J. Phys. C, Solid State Phys.* **1987**, *20*, 3469.

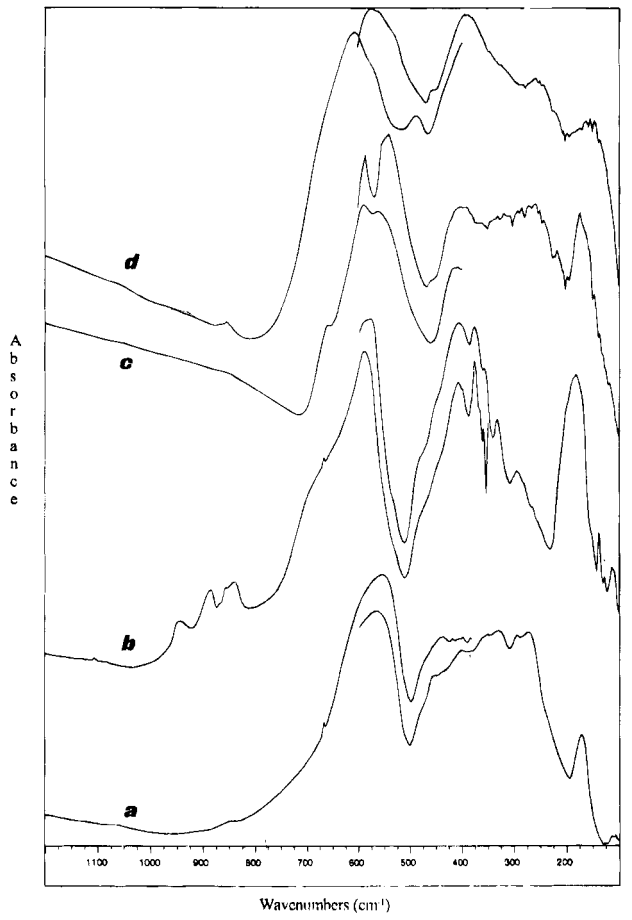

Figure 3. FT-IR/FT-FIR spectra of $LaFeO_3$ (a), $LaCrO_3$ (b), $LaCoO_3$ (c), and $LaMnO_3$ (d) samples, all calcined at 973 K. For any sample the medium-IR spectrum (KBr beam splitter and pressed disk) is superimposed to the far-IR spectrum (polyethylene beam splitter and pressed disk). The sharp peak at 667 cm^{-1} in spectra (a) and (b) is due to the deformation mode of gas-phase CO_2, unperfectly subtracted.

main absorptions in the regions 650–500 cm^{-1} (very intense), 450–250 cm^{-1} (with several maxima and components), and near 175 cm^{-1} (sharp).

According to the interpretation of the spectra of different perovskite phases, the first absorption arises from the $\nu 3$ IR-active vibrational mode of the perfect octahedral species MO_6 (F_{1u}) that is active and belongs to the same F_{1u} symmetry species also for the cubic perovskite structures. This mode is essentially an asymmetric M–O–M stretching. The loss of degeneracy upon lowering of the symmetry of the octahedron and the increase of the unit cell to more than one ABO_3 units cause this mode to split into several components, both IR and Raman active. In the case of the $LaCoO_3$ rhombohedral structure this mode gives rise to two IR-active components ($A_{2u} + E_u$), while in the $LaFeO_3$ orthorhombic structure it gives rise to five IR-active modes ($B_{1u} + 2B_{2u} + 2B_{3u}$). In effect, this band is clearly split in our $LaCoO_3$ spectrum (585, 550 cm^{-1}), while it appears as a broad almost componentless band in the cases of $LaCrO_3$ (585 cm^{-1}) and $LaFeO_3$ (560 cm^{-1}). The lack of multiplicity can just be due to the superposition of five bands very near each other. In the region 450–250 cm^{-1} the modes arising from the deformations of the MO_6 octahedra ($\nu 4$, F_{1u}, IR active and $\nu 6$, F_{2u}, inactive) are expected; they have the same symmetries and activities also in the case of cubic perovskites. These modes give rise to three IR-active modes for the rhombohedral phase ($A_{2u} + 2\ E_u$) and to 9 IR-active modes for the orthorhombic phase ($3B_{1u} + 3B_{2u} + 3B_{3u}$). We found here just three rather broad components in the spectrum of $LaCoO_3$ (410, 335, and 265 cm^{-1}) while in the cases of $LaFeO_3$ (351, 332, 297, and 276 cm^{-1}, with weaker components at 456, 402 cm^{-1}) and of $LaCrO_3$ (407, 375, 357 shoulder, 332, 295 cm^{-1}) a number of sharp peaks can be observed, with several other shoulders. The strongest bands obey the rule that for isostructural Fe(III) and Cr(III) compounds the bands of chromites are located 50–30 cm^{-1} above those of ferrites.

In the low-frequency region the modes arising from the La vibrational mode are expected (F_{1u} for a cubic perovskite). This mode gives rise to two IR-active modes for $LaCoO_3$ ($A_{2u} + E_u$) while to five modes for $LaFeO_3$ and $LaCrO_3$ ($B_{1u} + 2B_{2u} + 2B_{3u}$).

In effect we observe a sharp strong band in all three cases near 175–180 cm^{-1} but with additional sharp components at 138 and 115 cm^{-1} at least in the case of $LaCrO_3$.

The spectra we have recorded agree with those reported in the literature for the same compounds.[28–32] In Table 2 the maxima in our spectra are compared with those reported recently by Tajima et al.[31] in an IR reflectivity study of $LaFeO_3$ and $LaCoO_3$ monocrystals. It seems interesting to note that in that study only six of the eight IR-active fundamental modes of $LaCoO_3$ have been detected, as in our case. It can be noticed that the position of five of the six bands observed in our spectra almost perfectly coincide with those of the fundamental TO modes reported by Tajima et al.[31] Similarly, only six fundamentals of $LaFeO_3$ have been determined in that work and most of them are not far from the bands we observe here for the same compound.

Our spectra do not confirm the trend of the position of the highest frequency band in $LaMO_3$ phases with the change of M, discussed by Ganguly and Vasanthacharya[30] and its relation with octahedral field stabilization energy for the M cations.

So we can conclude that the spectra observed for the almost pure phases $LaFeO_3$, $LaCrO_3$, and $LaCoO_3$ very well agree with the structure determined by XRD.

However, the IR spectra also show the presence of impurities in our materials. The La_2CrO_6 impurity is responsible for weak peaks at 943, 885, and 840 cm^{-1} in the spectrum of $LaCrO_3$, associated to the Cr=O stretchings of the chromate ions, intrinsically very strong. In the spectrum of $LaCoO_3$ a shoulder at 660 cm^{-1} can be assigned to the spinel Co_3O_4 present as an impurity.[33]

The IR spectra show in all cases weak bands at 3610 and 650 cm^{-1}, which can be assigned to impurities arising from $La(OH)_3$ (OH stretching and deformations) and in the region 1500–1300 cm^{-1} due to carbonate species. These features are observed to be very strong in the spectra of La_2O_3 powders exposed to the ambient atmosphere[34] and can be considered as evidence that

(32) Wu, Yue; Yu, Zuolong; Liu, Shetian *J. Solid State Chem.* **1994**, *112*, 157.

(33) Busca, G.; Trifirò, F.; Vaccari, A. *Langmuir* **1990**, *6*, 1440.

(34) Andriamasinoro, D.; Kieffer, R.; Kiennemann, A.; Rehspringer, J. L.; Poix, P.; Vallet, A.; Lavalley, J. C. *J. Mater. Sci.* **1989**, *24*, 1757.

Table 2. Position (wavenumbers, cm^{-1}) of the IR Skeletal Bands in Some $LaMO_3$ Powders and Crystals[a]

$LaFeO_3$				$LaCoO_3$				$NdAlO_3$		
O monocrystal			$LaCrO_3$	R monocrystal			$LaMnO_3$	R monocrystal		$LaAlO_3$
TO	LO	powder	O powder	TO	LO	powder	R powder	TO	LO	R powder
				582	638	585	608	676	766	(740)
534	642	550	585	550	575	550	570	641	751	653
		456					480			
399	504	402	407	411	444	410		605	610	600
		351	375				395	499	623	530
316	466	332	357	328	370	330		435	498	432
278	398	297	332			265	250	420	573	422[b]
256	310	276	295	240	244			313	314	
164	190	177	181	174	192	174	180	196	274	254[b]
			138							
			115				150	160	268	185
ref 31		tw[c]	tw	ref 31		tw	tw	ref 38		tw

[a] O = orthorhombic; R = rhombohedral. [b] Possibly associated to La_2O_3 impurities. [c] tw = this work.

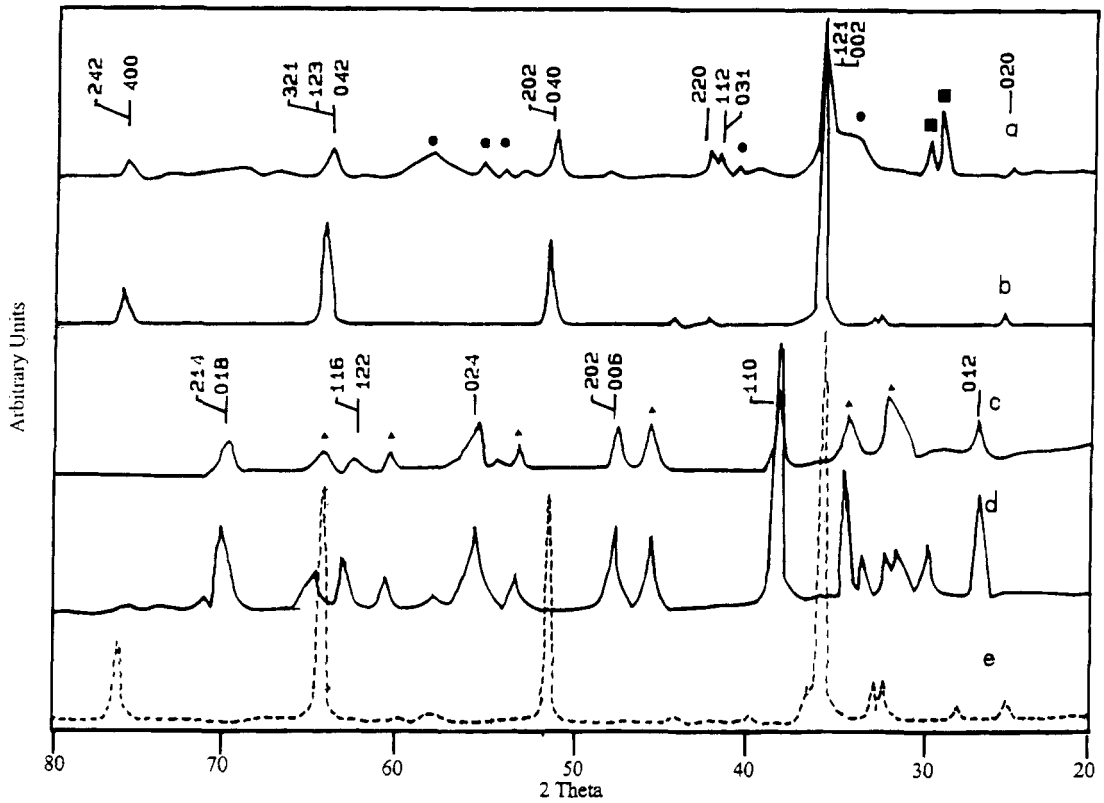

Figure 4. XRD patterns of $SrZrO_3$ calcined at 973 (a) and 1473 K (b) and of $LaAlO_3$ calcined at 973 K (c) and 1273 K (d). (e) Commercial $SrZrO_3$. The black squares represent the reflections attributed to $SrCO_3$, the circles the SrO peaks, and the triangles those of La_2O_3.

part of the lanthanum is not involved in the perovskite structure.

The IR spectrum of $LaMnO_3$ shows a very strong band in the Mn–O–Mn stretching region, weakly split at 608, 570 cm^{-1} (KBr pressed disks), evident bands at 480, 395, and 259 cm^{-1}, and more than one component in the range 180–150 cm^{-1}. In general, the spectrum of our $LaMnO_3$ sample looks broader and less defined than the previous ones. The splitting of the higher frequency band (with two components only partially resolved) and the low complexity of the 500–250 cm^{-1} region could be more in line with the rhombohedral oxygen-rich structure than with the orthorhombic stoichiometric phase. However, according to the XRD pattern, to the general broadness of the IR spectral features and to the multiplicity at low wavenumbers, it seems likely that the actual phase is weakly oxygen rich, with a coexistence or intergrowth of the orthorhombic and rhombohedral phases.

Characterization of $SrZrO_3$ and $LaAlO_3$. The XRD patterns of our $SrZrO_3$ preparation and of a commercial sample are compared in Figure 4. The sample calcined at 1473 K shows the features of a orthorombic perovskite phase, almost pure. We indexed it in the *Pnma* space group (the same of $LaFeO_3$), according to the JCPDS Table 10-268 and to Ahtee et al.,[35] although we cannot actually distinguish this structure from that proposed more recently by van Roosmalen et al.[36] for $SrZrO_3$, belonging to the $P2_13$ space group with $Z = 8$. It is evident that in the sample

(35) Ahtee, A.; Ahtee, M.; Glazer, A. M.; Hewat, A. W. *Acta Crystallogr.* **1976**, *B32*, 3243.
(36) van Roosmalen, J. A. M.; van Vlaanderen, P.; Cordfunke, E. H. P. *J. Solid State Chem.* **1992**, *101*, 59.

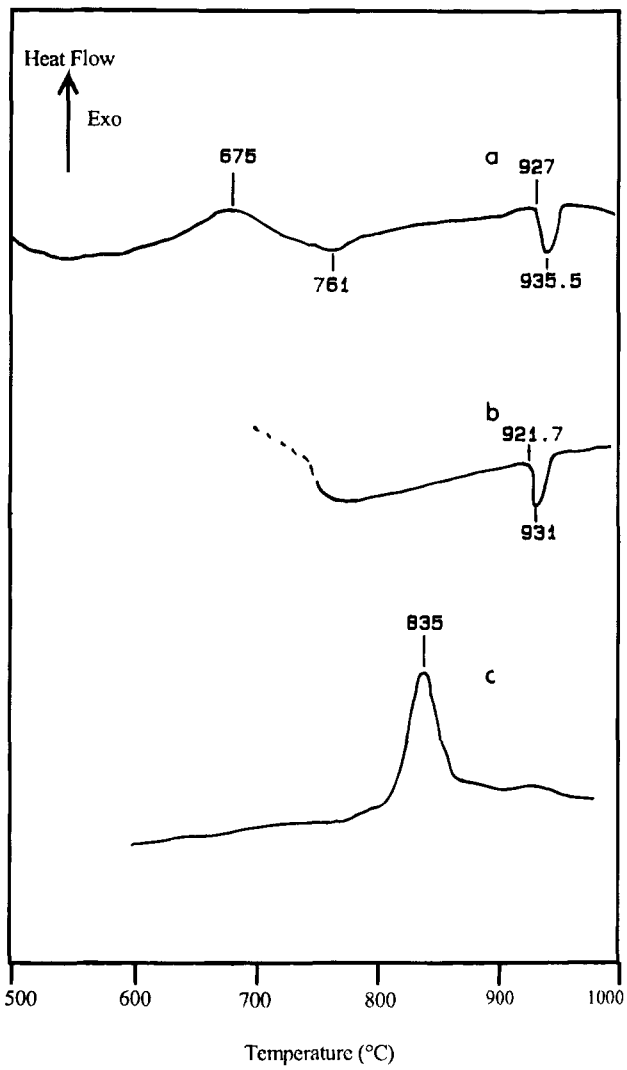

Figure 5. DTA curves relative to coprecipitated $SrZrO_3$ (a), $Sr_{0.9}La_{0.1}Zr_{0.9}Mn_{0.1}O_3$ (b), and $LaAlO_3$ (c).

calcined at 973 K, together with the main orthorhombic perovskite phase, impurities are present, easily identified as $SrCO_3$ and SrO (JCPDS Tables 5-0418, 6-0520).

The DTA plots of our $SrZrO_3$ specimens (Figure 5) show (after decomposition steps in the range up to 623 K) a broad exothermic peak assigned to the crystallization of the perovskite phase centered near 950 K with a corresponding small weight loss. Another small weight loss step is observed near 1030 K, corresponding to an endothermic peak in the DTA curve. These weight losses are likely associated with decomposition of carbonate species.

At higher temperatures a sharp endothermic peak is observed, with the onset at 1200 K and a maximum at 1208.5 K. A corresponding exothermic peak is found during cooling with a maximum at 1152.8 K. These features are typical of a reversible phase transition and can be assigned to the transition from the orthorhombic room temperature phase to a tetragonal phase (*I4/mcm* space group with $Z = 4$), characterized at 1173 K in static conditions (JCPDS Table 31-1366) or to a second orthorombic phase ($P2/n\bar{3}$ space group) as reported by van Roosmalen et al.[36] The same features, weaker and broader, appear in the DTA curves of the commercial $SrZrO_3$ sample, with a maximum of endothermic peak at 1205.5 K.

In Figure 6 the IR spectra of the commercial $SrZrO_3$ sample are compared with those of our preparation after calcination at 973 and 1473 K, respectively. We can assume[35] that the crystals belong to the same structure as $LaFeO_3$ (*Pnma* = D_{2h}^{16} space group, with $Z = 4$) so that the same considerations done above apply. However in this case four main absorptions are found. As discussed above, the higher frequency one is associated with the asymmetric stretching modes of Zr−O−Zr bonds and is observed in all cases in the 545−535 cm^{-1} range (KBr disks), with a shoulder, likely due to morphological components, near 680 cm^{-1}. In the medium-frequency region the absorptions due to the deformation modes of such bonds are expected. In this case the absorption is clearly split, but a difference is found from the spectrum of our low-temperature sample (where two broad bands are found with the maxima centered at 395 and 230 cm^{-1}, without clear evidence of other pronounced components) and the high-temperature samples (ours after calcination at 1473 K and the commercial one). In the latter cases, in fact, the maximum of the higher frequency component is at a distinctly lower frequency (330 and 342 cm^{-1}, respectively) with a pronounced shoulder at higher frequencies (380 cm^{-1}) and a third component near 365 cm^{-1}. As for the lower frequency component, absorptions near 285, 250, and 230 cm^{-1} are found in both high-temperature powders but with inverted intensity ratios.

The lowest frequency features are associated to the vibrations of the Sr^{2+} ion. For the high-temperature samples they are resolved in a main band, near 145 cm^{-1} (likely complex) and two sharper and weaker maxima at 122 and 106 cm^{-1}.

The spectra we observe compare well with those recorded on monocrystals by Perry et al.,[37] who found the main transverse optical modes at 552, 325, 240, and 143 cm^{-1}.

In Figure 4 the XRD patterns of our $LaAlO_3$ preparation are reported after calcination at both 973 and 1273 K. The perovskite-like $LaAlO_3$ phase (JCPDS Table 31-22) is detected, but La_2O_3 (JCPDS Table 5-0602) is also present in both cases in significant amounts. This parallels what has been reported by Lowe et al.,[14] who also obtained $LaAlO_3$ impure of La_2O_3 up to 1673 K. The discrepancy between element and phase composition (with La:Al 1:1, but with the copresence of $LaAlO_3$ and La_2O_3) in this sample implies that either $LaAlO_3$ solubilizes alumina, giving rise to a nonstoichiometric Al-excess phase, or that an XRD-undetectable alumina phase is also present. The first hypothesis can be ruled out by the observation that the unit cell parameters of the $LaAlO_3$ phase agree with those reported for stoichiometric samples. The IR spectrum of our $LaAlO_3$ sample (also reported in Figure 6) agrees with that reported in the literature[28] and can be interpreted on the basis of those reported in detail for monocrystals of the same $LaAlO_3$ and of $NdAlO_3$,[38] as done in Table 2. However, the presence of a broad absorption in the region 1000−700 cm^{-1} can be interpreted as evidence of the presence of amorphous or very poorly crystallized spinel-type alumina, likely stabilized by lanthanum, as

(37) Perry, C. H.; In *Far Infrared Spectroscopy*; Moller, K. D., Rothschild, W. G., Eds.; Wiley: New York, 1971; p 557.
(38) Alain, P.; Piriou, B. *Phys. Status Solidi* **1971**, *43*, 669.

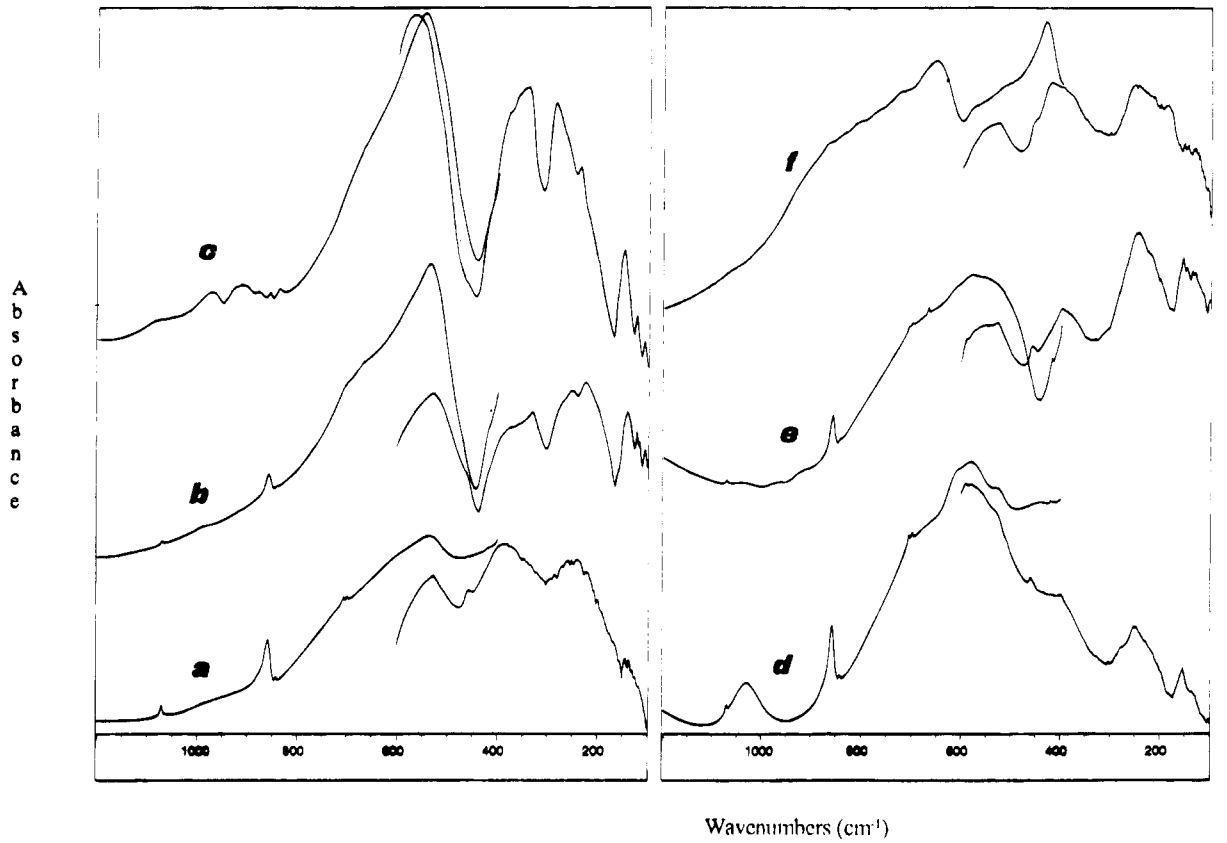

Figure 6. FT-IR/FT-FIR spectra of $SrZrO_3$ calcined at 973 K (a), $SrZrO_3$ calcined at 1473 K (b), commercial $SrZrO_3$ (c), $Sr_{0.9}La_{0.1}Zr_{0.9}Mn_{0.1}O_3$ calcined at 973 K (d), $Sr_{0.9}La_{0.1}Zr_{0.9}Mn_{0.1}O_3$ calcined at 1473 K (e), and $LaAlO_3$ calcined at 973 K (f). For any sample the medium IR spectrum (KBr beam splitter and pressed disk) is superimposed to the far-IR spectrum (polyethylene beam splitter and pressed disk).

reported in the literature.[39,40] Moreover, the La_2O_3 impurity can contribute to the bands near 420 and 250 cm^{-1}.[41,42]

Characterization of $La_xSr_{1-x}Mn_xZr_{1-x}O_3$ Solid Solutions. In Figure 7 the XRD patterns of the samples with compositions $Sr_{0.9}La_{0.1}Zr_{0.9}Mn_{0.1}O_3$ and $Sr_{0.75}La_{0.25}Zr_{0.75}Mn_{0.25}O_3$ after calcination at 973 and 1473 K are reported. The samples calcined at 1473 K show the pattern of the orthorhombic perovskite $SrZrO_3$. However, the unit cell parameters (Table 3) calculated from this pattern are definitely contracted, suggesting that a solid solution of the $SrZrO_3$ and $LaMnO_3$ phases has been obtained. On the other hand, the unit cell parameters measured on the two $La_xSr_{1-x}Mn_xZr_{1-x}O_3$ samples are almost identical despite the significantly different composition. Furthermore, the XRD pattern of the sample with $x = 0.25$ clearly shows also the most intense peaks of the $LaMnO_3$ phase. An evaluation of the phase composition of this sample based on the intensities of the most intense XRD peaks gives, for the mixed sample with $x = 0.25$, near 17% of $LaMnO_3$ as a separate phase. This indicates that the actual composition of the $La_xSr_{1-x}Mn_xZr_{1-x}O_3$ solid solution phase (evaluated in relation to the nominal $LaMnO_3$ amount and to the measured amount of this compound present as a separate phase) just corresponds to $x = 0.1$. We can consequently conclude that at 1473 K the solubility limit of $LaMnO_3$ in $SrZrO_3$ is near 10%. On the other hand, by applying the Vegard's law[19] to the data we obtained for orthorhombic $LaMnO_3$ and $SrZrO_3$, the calculated solubility of $LaMnO_3$ in $SrZrO_3$ does not exceed 5% if the a and b axes are taken into account, but it can as high as 12% if the c axis is taken into account.

The contraction of the unit cell agrees with the definitely smaller size of octahedrally coordinated Mn^{3+} (0.58–0.66 Å, following different authors)[43] with respect to octahedrally coordinated Zr^{4+} (0.72–0.80 Å)[43], in contrast to the similar sizes of Sr^{2+} and La^{3+}.

On the other hand, the cell of the $LaMnO_3$ minority phase appears to be slightly but significantly enlarged in the sample with $x = 0.75$. The cell parameters calculated from our experimental pattern are $a = 5.528(2)$ Å and $c = 13.501(8)$ Å, assuming an orthorhombic structure, showing that the c parameter is slightly enhanced with respect to the pure $LaMnO_3$ sample (Table 1). This suggests that part of $SrZrO_3$ is solubilized in $LaMnO_3$.

The samples calcined at 973 K are poorly crystalline, in contrast to the partial crystallinity of the "pure" $SrZrO_3$ sample after the same treatment. This can be interpreted as an evidence of the difficulty in the formation of this solid solution, possibly related to the significantly different sizes of Mn and Zr cations that is also reflected in the relatively small solubility.

(39) Zhang, H. M.; Teraoka, Y.; Yamazoe, N. *Catal. Today* **1989**, *6*, 155.
(40) Wachowski, L.; Kirzensztejn, P.; Lopatka, R.; Czajka, B. *Mater. Chem. Phys.* **1994**, *37*, 29.
(41) McDevitt, N. T.; Baun, W. L. *Spectrochim. Acta* **1964**, *20*, 799.
(42) Boldish, S. T.; White, W. B. *Spectrochim. Acta* **1979**, *354*, 1235.
(43) Moeller, T. *Inorganic Chemistry, a Modern Introduction*; Wiley: New York, 1982; p 141.

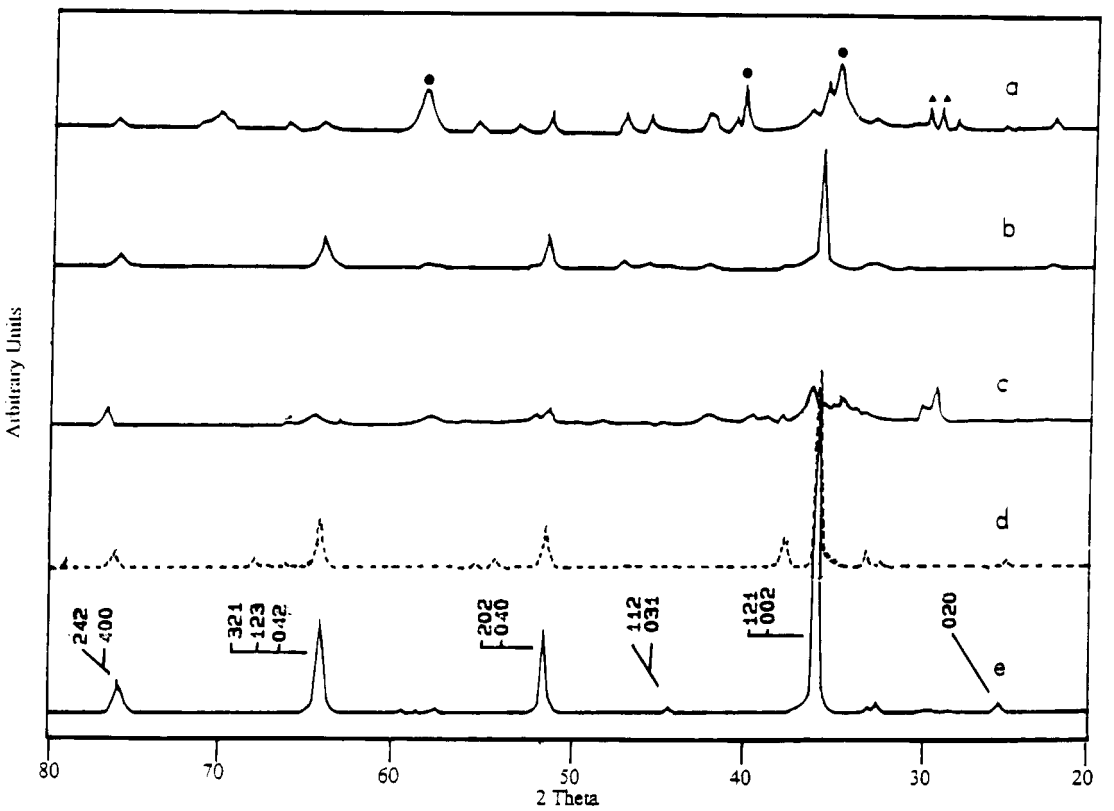

Figure 7. XRD patterns of $Sr_{0.9}La_{0.1}Zr_{0.9}Mn_{0.1}O_3$ calcined at 973 K (a), calcined at 1473 K (b), $Sr_{0.75}La_{0.25}Zr_{0.75}Mn_{0.25}O_3$ calcined at 973 K (c), calcined at 1473 K (d), $SrZrO_3$ calcined at 1473 K (e). The triangles show the main reflections of $SrCO_3$, while the circles those of SrO.

Table 3. Space Group, Cell Parameters, and Phases of $SrZrO_3$: Series Samples

sample	calcination temp (K) (time (h))	space group	XRD phase	cell parameters (Å)			impurities	ref
				a	*b*	*c*		
$SrZrO_3$	973 (3)	*Pnma* D_{2h}^{16} $z = 4$	O	5.815 (3)	8.204 (7)	5.809 (5)	$SrCO_3$	tw[a]
	1473 (3)	*Pnma* D_{2h}^{16} $z = 4$	O	5.813 (2)	8.224 (4)	5.816 (4)		tw
commercial		*Pnma* D_{2h}^{16} $z = 4$	O	5.804 (0)	8.207 (1)	5.805 (0)	SrCO3	tw
		Pnma D_{2h}^{16} $z = 4$	O	5.814	8.196	5.792		*b*
$Sr_{0.9}La_{0.1}Zr_{0.9}Mn_{0.1}O_3$	973 (3)	*Pnma* D_{2h}^{16} $z = 4$	O	5.821 (3)	8.193 (9)	5.792 (6)	$La_2CO_5 + SrO + SrCO_3$	tw
	1473 (3)	*Pnma* D_{2h}^{16} $z = 4$	O	5.800 (2)	8.206 (5)	5.804 (4)		tw
$Sr_{0.75}La_{0.25}Zr_{0.75}Mn_{0.25}O_3$	973 (3)	*Pnma* D_{2h}^{16} $z = 4$	O	5.797 (5)	8.207 (16)	5.776 (10)	$La_2CO_5 + SrCO_3$	tw
	1473 (3)	*Pnma* D_{2h}^{16} $z = 4$	O	5.799 (2)	8.207 (6)	5.800 (4)	$LaMnO_3$	tw

[a] tw = this work. [b] JCPDS Table 10-268.

The DTA curves of the two mixed samples show the perovskitic phase transition already observed for pure $SrZrO_3$ but shifted in both cases at slightly lower temperatures (onset 921.7 °C/1194.7 K, peak 931 °C/1204 K; Figure 5b for $x = 0.1$).

The skeletal IR spectrum of the sample with $x = 0.1$ after calcination at 1473 K (Figure 6), i.e., of the nearly pure saturated solid solution, is similar to that of pure $SrZrO_3$ but is definitely less resolved. This can be associated to the random cation distribution in this solid, with the possible additional effect of cation vacancies associated to an oxygen excess typical of Mn^{3+} compounds, as already discussed for $LaMnO_3$.

Morphology Characterization: Surface Areas and Crystal Sizes. In Table 4 the BET surface areas and the crystal sizes of our materials are reported, after calcination at 973 K. It seems evident that the surface areas of all materials after this treatment do not exceed 10 m^2/g, except for the $LaFeO_3$ aerogel and the two potential supports $SrZrO_3$ and $LaAlO_3$, that lie in the range 10–20 m^2/g. The surface areas ranges we found for $LaMnO_3$ and $LaCoO_3$ agree with those reported in several literature papers[9–13,44–47] and reflect the relatively high heating temperature needed to crystallize

(44) Duprat, A. M.; Alphonse, P.; Sarda, C.; Rousset, A.; Gillot, B. *Mater. Chem. Phys.* **1994**, *37*, 76.
(45) Sundar Manoharan, S.; Patil, K. C. *J. Solid State Chem.* **1993**, *102*, 267.
(46) Tijburg, I. I. M.; Geus, J. W.; Zandbergen, H. W. *J. Mater. Sci.* **1991**, *26*, 6479.

Table 4. Crystal Sizes Theoretical and Experimental Surface Areas of All the Samples

sample	calcination temp (K) (time (h))	theor surf. area (m^2/g)[a]	exper surf. area (m^2/g)	crystal size (Å)
$LaFeO_3$	973 (1.5)	56	19	161
$LaCrO_3$	973 (1.5)	25	6	358
$LaMnO_3$	973 (3)	77	7	343
$LaCoO_3$	973 (3)	116	8	215
$LaAlO_3$	973 (3)	100	18	277
$SrZrO_3$	973 (3)	46	12	240
	1473 (3)	34	5	320
commercial		34	3	323
$Sr_{0.9}La_{0.1}Zr_{0.9}Mn_{0.1}O_3$	973 (3)	108	4	101
	1473 (3)	37	1	295
$Sr_{0.75}La_{0.25}Zr_{0.75}Mn_{0.25}O_3$	973 (3)	57	7	192
	1473 (3)	62	2	349

[a] Calculated from the crystal diameter measured with the Scherrer's method, assuming a spherical particle.

these phases and the relatively weak resistance of these materials to sintering.

The resistance to sintering of our $LaAlO_3$ (that is actually not the pure phase and likely contains La-stabilized alumina) is stronger than for the isostructural transition metal-based compounds. However, the areas obtained, although much higher than those reported for $LaAlO_3$ "fine powders",[48] agree with those reported by Lowe[14] being by far smaller than those that can be obtained using aluminas doped with small amounts of La[15,39,40] or using the β-alumina phase $LaAl_{11}O_{18}$, which is reported to still retain more than 100 m^2/g after heating 4 h at 1273 K.[14]

The data we found for $SrZrO_3$ are comparable but smaller than those reported by Lowe et al.[14] It seems evident that this material, without modification, is too weakly resistant to sintering to allow its use as a support in the case of high-temperature combustion catalysis. Moreover, the mixing of $SrZrO_3$ to $LaMnO_3$ (at least in the $SrZrO_3$-rich region) does not seem to have any positive effect as the surface area of the catalyst is concerned.

In Figure 8 the SEM micrographs of the two aerogel samples $LaCrO_3$ and $LaFeO_3$ and of one of our coprecipitated samples, $LaMnO_3$ are compared. The two aerogel samples are composed of well-defined particles, spherical in the case of the chromite, less symmetrical for the ferrite, whose diameter is of the order of one to a few microns. This value is nearly 100 times larger than the crystal size evaluated from the XRD line broadening (Table 4). So, the particles observed by SEM are obviously aggregates of smaller crystals. This is also confirmed by the IR spectra of the pure powders (see below) that in fact show very limited radiation scattering, so implying a particle size definitely smaller than the IR light wavelength (well below 1 μm). On the other hand, if the measured surface area, e.g., of $LaCrO_3$, is taken into account, we can easily calculate a particle size (assuming spherical particles) of no more than 0.15 μm. This indicates that the spherical particles appearing to SEM are porous and that "internal" surface participates to the total surface area.

The coprecipitated samples appear to the SEM analysis to be composed by much less defined big spongelike particles aggregates, while information on the shape and size of individual crystals could not be obtained.

Surface Characterization by IR Spectroscopy. The surface structure of the perovskite-type compounds has been investigated by IR spectroscopy. The spectra of the pure pressed disks of all compounds show strong bands in the region 1600−1200 cm^{-1}, associated with the C−O stretchings surface carbonates. Additional weaker bands are found near 2500, 2400, and 1060 cm^{-1} and in the 1800−1720 cm^{-1} region, due to other absorptions of carbonate bands (overtone, combinations, and Raman-active modes).[18] Outgassing at temperatures up to 1073 K causes only the partial decrease in intensity of these absorptions, while adsorption of CO_2 at room temperature causes their complete restoration. This behavior is typical of basic surfaces, where partially uncoordinated oxide ions characterized by strong nucleophilicity are available to attack the cation atom of CO_2 giving rise to stable surface carbonates. A more detailed analysis of the absorptions due to carbonate species allow us to distinguish in all cases different coordination states for the CO_3^{2-} ion, such as bidentate, bridging, and nearly symmetrical ions. A study of carbonated lanthana and of lanthanum oxycarbonate shows that these phases only partly contribute to the carbonates spectrum, if any. So, most of the observed bands should be related to adsorbed carbonate species. This behavior characterizes all the present phases as definitely basic materials.

To have a confirmation on the characteristics of such surfaces, we have investigated also the IR spectra of adsorbed pyridine over them. The spectra found over $LaCrO_3$, $LaFeO_3$, and $SrZrO_3$ are reported in Figure 9. They are representative of those we have found also over the $LaCoO_3$ and $LaMnO_3$ catalysts, although in these cases the noise is very high due to the partial opacity of the samples to the IR radiation. As is well-known, some bands of pyridine are sensitive to the strength of the coordinative interaction involving the nitrogen lone pair. The most sensitive bands are the so-called 8a, 19b, and 1 modes, which are observed in liquid pyridine at 1580, 1438, and 992 cm^{-1},[49] and all tend to shift up the more, the stronger is the interaction. The 19b mode is in our case superimposed on the carbonate bands. So, its position for adsorbed pyridine cannot be determined precisely. The other modes for pyridine adsorbed at room temperature on our perovskite samples are found in the ranges 1602−1596 cm^{-1} (band 8a) and at 1004−1000 cm^{-1} (band 1) in all cases and do not shift significantly by outgassing. These data do not disagree

(47) Simonot, L.; Garin, F.; Maire, G.; Poix, P.; In *Preprints of the VIth Int. Symp. on Preparation of Catalysts*; Louvain la Neuve, Belgium, 1994; Vol. 2, p 251.

(48) Kingsley, J. J.; Suresh, K.; Patil, K. C. *J. Solid State Chem.* **1990**, *87*, 435.

(49) Corrsin, L.; Fax, B. J.; Lord, R. C. *J. Chem. Phys.* **1953**, *21*, 1170.

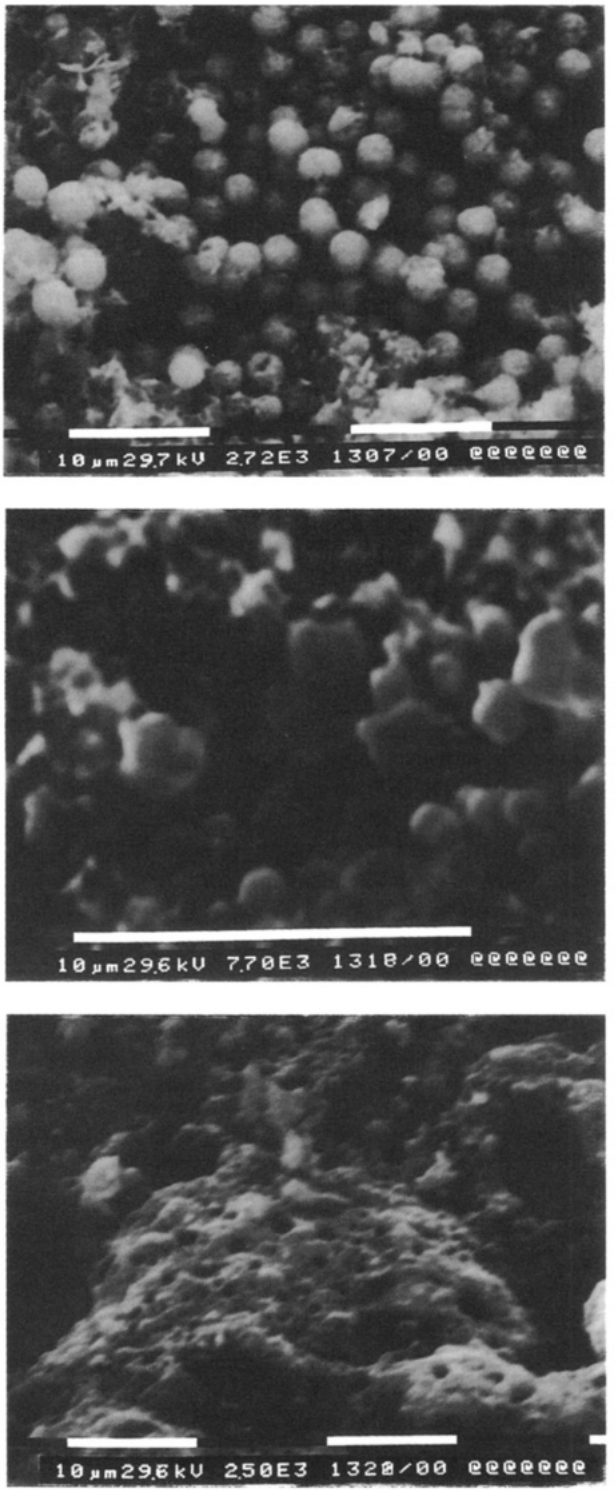

Figure 8. SEM photographs of $LaCrO_3$ (a, top), $LaFeO_3$ (b, middle), and $LaMnO_3$ (c, bottom), all calcined at 973 K. Magnification: (a) 2720; (b) 7700; (c) 2500.

substantially with those reported by Tascon et al.[16] although the Brønsted acidity found by these authors, in contrast with our data, is likely associated to water impurities in the pyridine. The positions of the bands we observe here is similar to those observed by us over other perovskite samples like $BaTiO_3$[18] and $SrTiO_3$[50] and characterize all these materials as very weakly acidic solids. This datum confirms that these are typically strongly basic materials. Perovskites like

(50) Unpublished results from this laboratory.

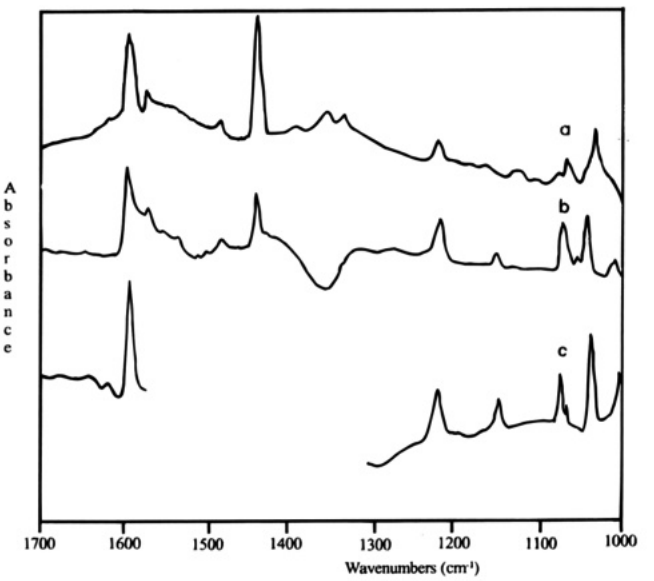

Figure 9. FT-IR spectra of pyridine adsorbed on $LaCrO_3$ (a), $LaFeO_3$ (b), and $SrZrO_3$ (c) (a part of the last spectrum is masked by carbonates impurities).

$LaFeO_3$ and $LaCrO_3$ are definitely more basic and less acidic compared to the corresponding pure oxides Fe_2O_3 and Cr_2O_3 and the corresponding spinel-type compounds like $MgFe_2O_4$ and $MgCr_2O_4$.[51]

The basic character of all these perovskite powders can be interpreted considering the main features of the ABO_3 perovskite-like structure that is generated only if the A cation has a sufficiently big size. In these structures the oxide anions have only two coordinations with the rather small and rather strongly polarizing B cations, while they are certainly only weakly polarized by the very big A cations. When these oxide ions lie at the surface, they are coordinatively unsaturated and their coordination with B cations is likely lowered to one. So, the surface anions on perovskite surfaces are by far less polarized than over other mixed oxide surfaces, like the spinels AB_2O_4, where they are coordinated by three B cations and one A cation that, incidentally, is also much smaller and more polarizing than in the case of the A cations in perovskites.

Conclusions

The main conclusions from the present work are the following:

$LaMO_3$ perovskite-type phases can be obtained either through the supercritical drying method or through a conventional coprecipitation technique only after calcination at 773 or 973 K. A similar coprecipitation procedure gives rise to $SrZrO_3$.

XRD and IR skeletal analyses show that the structure of the materials obtained corresponds to that reported for powders prepared by solid-state reactions, with orthorhombic perovskite for $LaFeO_3$, $LaCrO_3$, and $SrZrO_3$, rhombohedral perovskite for $LaCoO_3$ and an intermediate phase due to an oxygen excess for $LaMnO_{3+x}$.

Due to the high-temperature treatments necessary for the crystallization of these phases, the resulting surface areas are in all cases not exceeding the range 10−20

(51) Busca, G.; Lorenzelli, V.; Ramis, G.; Willey, R. J. *Langmuir* **1993**, *9*, 1492.

m^2/g after calcination at 973 K. $LaAlO_3$ and $SrZrO_3$ powders do not seem to be sufficiently resistant to sintering and cannot be used as supports for high-temperature catalytic combustion catalysts.

SEM analyses show that aerogel materials are characterized by well defined almost spherical homogeneous aggregates while coprecipitated samples are constituted spongelike aggregates.

With similar methods the preparation of solid solution phases of composition $La_xSr_{1-x}Mn_xZr_{1-x}O_3$ has been attempted. However, the materials after calcination at 973 K are, in this case, poorly crystallized. After calcination at 1473 K, instead, the solid solution can be obtained well crystallized.

It has been found that solubility of $LaMnO_3$ into $SrZrO_3$ does not exceed 10% after calcination at 1473 K.

All these materials, like other perovskite compounds studied previously, appear to have a predominant surface basic character.

Acknowledgment. This work has been supported in part by MURST, Rome, Italy, and by NATO, CRG 900463.

CM950194V